Compact Fiber Fabry–Perot Sensors filled with PNIPAM hydrogel for highly Sensitive Relative Humidity Measurement

Ru-Lei Xia,[1] Juan Liu,[1] Jiulin Shi,[1] Xing-Dao He,[1] Jinhui Yuan,[3] Andrew R. Pike,[4] Liang Chu,[5] Qiang Wu[1,2,*] and Bin Liu[1,*]

[1]*Key Laboratory of Opto-Electronic Information Science and Technology of Jiangxi Province, Nanchang Hangkong University, Nanchang 330063, China*

[2]*Faculty of Engineering and Environment, Northumbria University, Newcastle Upon Tyne, NE1 8ST, United Kingdom*

[3]*Research Center for Convergence Networks and Ubiquitous Services, University of Science & Technology Beijing, Beijing 100083, China*

[4]*School of Chemistry, Newcastle University, Newcastle Upon Tyne, NE1 7RU, United Kingdom*

[5]*School Electronics and Information, Hangzhou Dianzi University, Hangzhou 310018, China*

** Corresponding authors: liubin_d@126.com; qiang.wu@northumbria.ac.uk*

Abstract

A fiber-optic Fabry–Perot (FP) based relative humidity (RH) sensor was proposed and experimentally investigated by using Poly(N-isopropylacrylamide) (PNIPAM) hydrogel to connect two ends of single-mode optical fiber to formulate a PNIPAM FP cavity. The water vapor will be absorbed by the PNIPAM hydrogel, which will alter both the refractive index (RI) and dimension of the PNIPAM FP cavity, resulting in the change of output resonance intensity in the reflective spectrum. The measure RH sensitivity is 1.634 nm/%RH within RH range from 45-75% with good linearity of 0.9897 and excellent repeatability. The influence of PNIPAM hydrogel concentration on the RH sensitivity has been investigated - the higher the concentration of PNIPAM hydrogel, the higher the RH sensitivity of the sensor. The developed sensor can effectively monitor human respiratory with response and recovery time of 0.91 s and 1.91 s, respectively.

Keywords: Fiber-optic sensor; PNIPAM hydrogel; Fabry-Perot interferometer (FPI); Relative humidity (RH);

1. Introduction

Human survival and social activities are closely related to RH. RH sensors are broadly used in aerospace, electrical power, military, tobacco, industrial control, pharmaceutical production, agricultural planting, weather detection and food storage and other departments, often need to measure and control environmental humidity. Traditional humidity sensor types include hair type, wet and dry bulb type, capacitive type, and resistance type humidity sensors. These types of humidity sensors are susceptible to interference from electromagnetic, oil and gas and other harsh environments, which have poor stability and limited application range. Optical fiber sensor is a passive sensor, which is not easily interfered by electromagnetic signals, and is intrinsically safe (flame retardant, explosion-proof), and can be adapted to flammable and explosive environments such as electrical power, chemical

industry and pharmaceuticals. In addition, the optical fiber sensor is small in size and light in weight, and it is easier to be placed in a small space for long-distance network monitoring. In order to detect RH, fiber optic humidity sensors are fabricated, which can be roughly achieved by forming FPI on the fiber end face and coating the fiber surface with hydrophilic materials. These include swelling effects based on hydrophilic materials such as polyvinyl alcohol (PVA)[1], poly (ethylene oxide) (PEO) [2], Nafion®[3], polymer microrods[4] and whole agar[5]. In the swelling effect, the dimension of the hydrophilous material will swell with the change of RH. In general, hydrophilic materials are coated on some particular sensor structures such as U-shaped panda polarization-preserving microfibers[6], Fabry-Perot interferometers [7], fiber Bragg gratings[8], single-mode multimode single-mode[9][10] and a mismatched fused Mach-Zehnder interferometer[11] to convert changes in ambient RH into deformations in the sensor structure. For example, FPI was formed as sensing systems by filling the pores of special microstructured optical fibers (MOFs) with chitosan as a sensing material[12]. In 2019, Yunlong Wang *et al*[13] proposed a fiber-optic RH sensor that coats the prepared PEG/PVA composite film on long-period fiber grating (LPFG). The sensor has a sensitivity of 2.485 nm/%RH in the 50-75% RH range. In 2020, Xiaoting Sun *et al*[14] studied a Michelson interferometer all-fiber RH sensor composed of a thin-core optical fiber (TOF) structure coated with a hyaluronic acid (HA) and polyvinyl alcohol (PVA) composite film. The maximum sensitivity of the sensor is −0.1679 nm/%RH. In 2021, Ziwan Li *et al*[15] proposed a FBG humidity sensor based on polyimide and graphene films. In the humidity range of 30%~70%RH, its sensitivity is calculated to be 19.8 pm/%RH.

Combining the above studies, we designed and validated a fiber-optic RH sensor comprising a PNIPAM hydrogel FPI. PNIPAM hydrogel was discovered as hygroscopic material utilizing hydrophilic amido groups on the macromolecular chains. Therefore, with increasing RH, water molecules can be absorbed by the PNIPAM hydrogel, thereby changing its refractive index (RI) and volume, and resulting in a shift in the reflectance spectrum of the fiber-optic FPI RH sensor. The RH response characteristics of the sensors at different PNIPAM concentrations were studied and the repeatability of the sensor and the respiratory response and recovery time were investigated.

2. Material and methods

As shown in Fig. 1(a), the PNIPAM was manufactured as follows:

i. Weigh 10g N-isopropylacrylamide monomer and 50mL benzene;
ii. Put the weighed drug in a 100mL three-neck bottle, add an initiator AIBN equivalent to 1% of the monomer substance, and reflux for 10h in a 65°C constant temperature water bath under nitrogen protection;
iii. The reflux product is evaporated to remove benzene and dissolved with a small amount of acetone, and then dropwise into n-hexane;
iv. After suction filtration, dry under vacuum at 30°C for 48h to obtain a white solid of poly-N-isopropylacrylamide which is easily soluble in polar solvents such as water and ethanol;
v. Finally, PNIPAM hydrogels were successfully fabricated by dissolving the solids in deionized water. The number average molecular mass measured by Agilent 1100 series gel chromatograph was 1.65×10^4g/mol.

In order to more clearly see the binding process of PNIPAM hydrogels and water molecules, a model of the impact of the process was presented and showed in Fig. 1(b)[26]. In short, at a relatively low temperature(20℃), there are a large number of NH hydrophilic groups in the interior of the PNIPAM hydrogel, and it is the existence of these hydrophilic groups that makes the PNIPAM hydrogel have the ability to adsorb water molecules. Because there are a large number of hydrophilic groups in the hydrogel, these groups and polar water molecules attract each other through hydrogen bonding, and the water molecules in the air are firmly adsorbed inside the PNIPAM hydrogel. The first layer of water molecules and hydrophilic groups attract each other

through hydrogen bonding to fix the water molecules on the molecular chain, and then the water molecules are adsorbed on the polymer chain layer by layer through van der Waals force. That is to say, the existence of a large number of NH hydrophilic groups in the PNIPAM hydrogel, the water molecules in the air are firstly fixed in the hydrogel layer by layer through chemical adsorption and then physical adsorption. Due to the molecular motion, when the water molecules are adsorbed and dissipated to the air at the same rate, the water absorption of the hydrogel reaches a dynamic equilibrium. When the external humidity increases, the hydrogel will continue to absorb water molecules [16].

Dr. Priyanka Dey *et al*, proposed the use of the polymer PNIPAM to control the poly(sodium acrylate)(PSA) polymer conformation to improve the efficiency of the forward osmosis (FO). The polymer chains are extended and the large number of the hydrophilous groups on the polymer are conducive to increase the rate of water flow [17].

Yuanyuan Pan *et al*, propose that a novel nano-porous membrane with multi-wall carbon nanotubes (MWCNTs) filled with PNIPAM hydrogel. The improved hydrophilicity of the hydrogel-filled nanochannels is hopeful of facilitating the movement and transport of aqueous solutions[18].

Zheng-wei Dai *et al*, proposed the preparation of polyurethane (PU) and PNIPAM semi-interpenetrating network polymer (semi-IPN) into micro-porous films by submersion sediment phase inversion way. The introduction of PNIPAM greatly improved the hydrophilicity, water absorption and moisture permeability of the membrane. [19].

These schemes demonstrate the promising future application of fiber-optic humidity sensors by exploiting the hydrophilicity of PNIPAM hydrogel, which have the potential for using in the water industry and biological tissue engineering [20-22].

Figure 2(a) shows a schematic diagram of the manufacturing process of the optical fiber RH sensor, which can be divided into three steps. First, a SMF was cleaved into two sections and then place the two flat-cut SMFs on both sides of the three-dimensional (3D) translation stage. Second, use the 3D translation stage to align the two SMF ends to form a desired gap. Finally, Drop the PNIPAM hydrogel on the gap of the two SMF ends and leave it at room temperature for 12 hours to cure. Figure 2(b) shows the microscope picture of a fabricated optical fiber PNIPAM hydrogel FPI. In addition, the distal end of the SMF was angularly cleaved and roughed by sandpaper to suppress reflection, which avoid dense spectrum fringe coming from the SMF FPI.

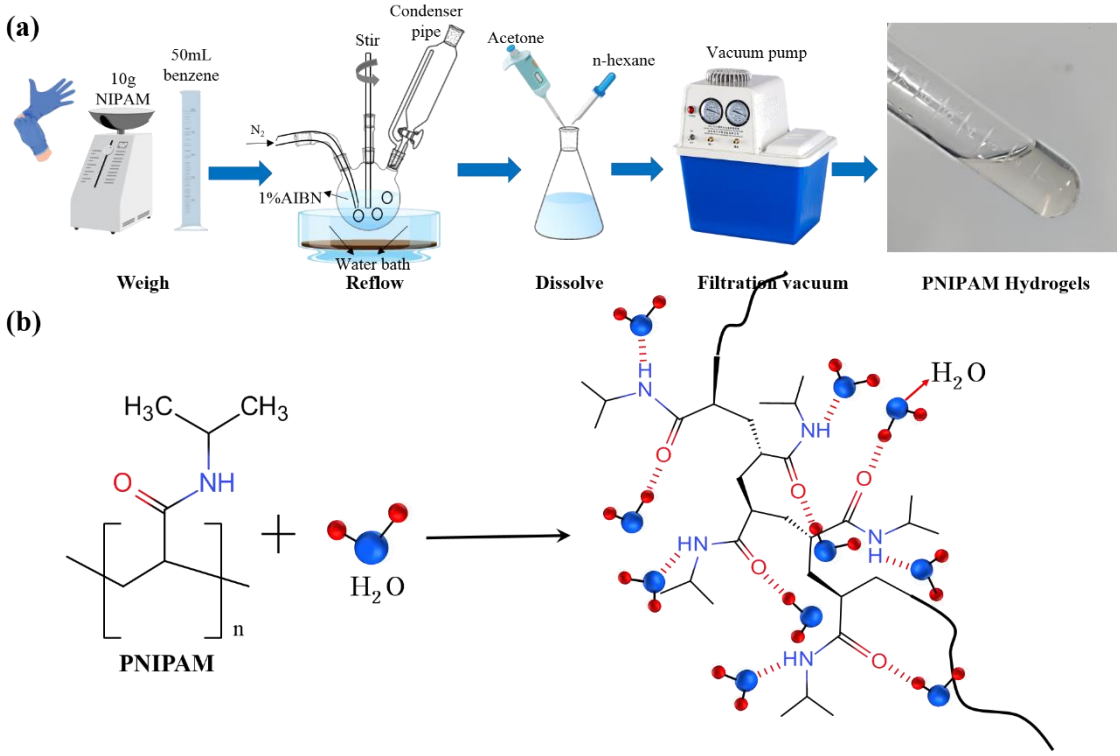

Fig. 1 (a) Schematic diagram of the fabrication process of PNIPAM hydrogel; (b) A model of the binding process for PNIPAM hydrogels and water molecules.

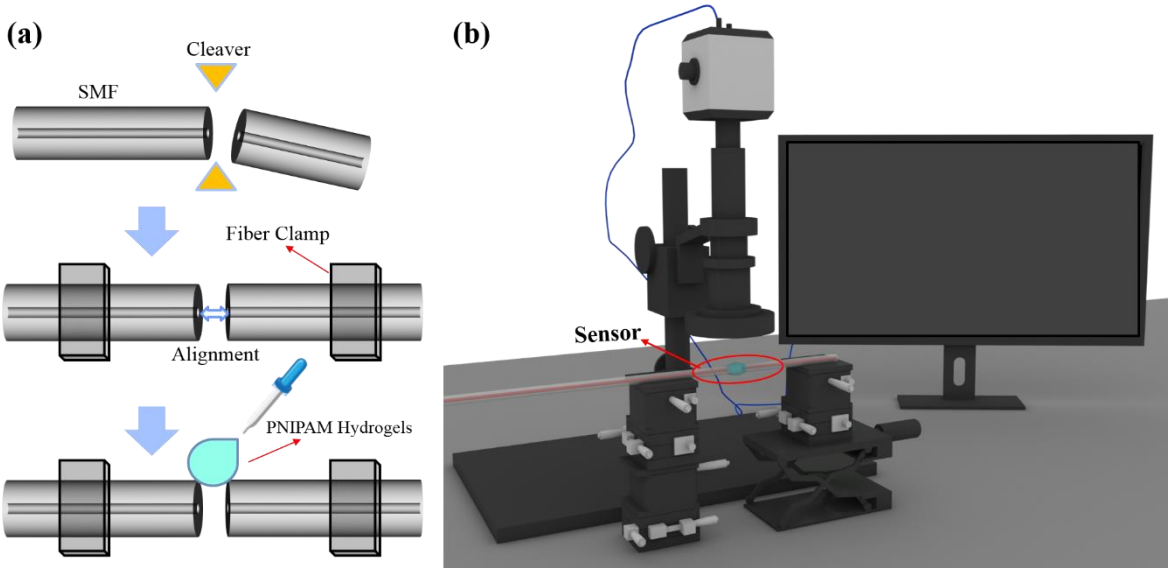

Fig. 2 (a) Three manufacturing steps of the sensor: cutting flat; alignment; dripping; (b) Diagram of the equipment for making the completed sensor structure.

3. Theoretical background

The schematic diagram of the proposed sensor structure and reflection model is shown in Fig. 3(a), which consists of two single-mode fibers (SMFs，SMF-28e) with a gap filled with PNIPAM to form a FP cavity. The core diameter and the external diameter of the SMF used in experiment is ~9 μm and ~125 μm. Figure 3(b) shows a microscope picture of the fabricated FPI structure filled with PNIPAM hydrogel.

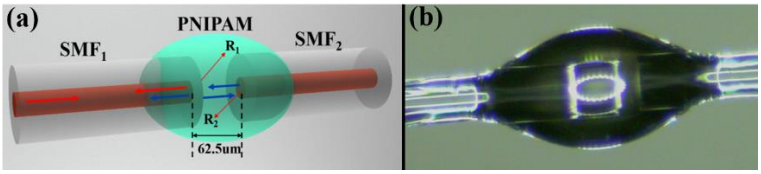

Fig. 3(a) Schematic diagram of the reflection model; (b) Microscopic picture of the fabricated FPI structure filled with PNIPAM hydrogel.

As shown in Fig. 1(a), the reflection coefficients of the two interfaces in the FP cavity are defined as R_1 and R_2, representing the reflexion coefficient at the port between SMF_1 and PNIPAM hydrogel (R_1) and the interface before PNIPAM hydrogel and SMF_2 (R_2), respectively. Assuming the reflection coefficient $R_1 = R_2 = R$ and the RI of the FP cavity filled with PNIPAM hydrogel is n, the reflected light intensity I_r can be defined as[23]:

$$I_r = \frac{2R[1 - cos(4\pi nL/\lambda)]}{1 + R^2 - 2Rcos(4\pi nd/\lambda)} I_0 \quad (1)$$

where L represents the FP cavity length, λ represents the wavelength, and I_0 represents the intensity of the input light. Assuming that the reflection coefficient R is relatively low (≈4%), it can be deduced that the reflected light intensity I_r is：

$$I_r = 2R[1 - cos(4\pi nL\lambda)]I_0 \quad (2)$$

Water molecules can be absorbed by the hydrophilic amide groups on the macromolecular chain of PNIPAM hydrogel, which will introduce changes of both RI and FP cavity length, which can be expressed as:

$$\Delta\delta = 2(\Delta n_e L + n_e \Delta L) = \delta\left(\frac{\Delta n_e}{n_e} + \frac{\Delta L}{L}\right) \tag{3}$$

where n_e represents the effective RI of PNIPAM hydrogel, δ represents the optical path difference of the FP cavity.

After the water molecule is adsorbed on PNIPAM hydrogel, its volume will increase according to the law of volume addition and thus the variation in the cavity length ΔL is related to the PNIPAM hydrogel swelling effect [24]:

$$\frac{\Delta L}{L} = \frac{1}{\gamma}\frac{\Phi_w}{1-\Phi_w} \tag{4}$$

$$\Phi_w = \Phi_{wm}\frac{KC}{1+KC} \tag{5}$$

Here, γ is moisture concentration, when γ =1, it means axial swelling. Φ_w represents the adsorbing amount of water molecules by the PNIPAM hydrogel and Φ_{wm} represents the largest adsorbing amount. K represents the counterpoise constant adsorbing capacity and C represents the density of water molecules.

Due to the connection between the water vapor density and wavelength shift can be defined as $\Delta\lambda \propto \Delta n \propto \Delta C$,[25] the RI of the PNIPAM hydrogel is in direct ratio to water absorption. With the increase of RH, water molecules are continuously absorbed by PNIPAM hydrogel, which results in increasing RI and cavity length, and the reflection spectrum shifts to long wavelengths, i.e., red-shifts. The relative wavelength shift can be calculated as:

$$\frac{\Delta\lambda}{\lambda} = \Delta RH\left(\frac{1}{n_e}\frac{dn_e}{dRH} + \frac{1}{L}\frac{dL}{dRH}\right) \tag{6}$$

On the whole, with the increase of RH, water molecules are continuously absorbed by PNIPAM hydrogel, which results in increasing RI and the optical path difference of the FP cavity, and the reflection spectrum shifts to long wavelengths, i.e., red-shifts. The lower the concentration of PNIPAM hydrogel, the less water molecules adsorb the external environment, and the lower the sensitivity of the sensor.

4. Experimental results and analysis

The schematic diagram of the experimental devices are shown in Fig 4(a), which is constituted with a broadband light source (BBS, MAX-RAY PHOTONICS C+L ASE Source), an optical fiber circulator (OC), the fiber sensor probe, an optical spectrum analyzer (OSA, YOKOGAWA AQ6370D), and an adjustable constant temperature and humidity chamber (ST-80L), which can change the RH of surrounding from 45% to 75%. In short, at a relatively low temperature(20℃), PNIPAM hydrogel can be well combined with the water molecules in the humidity chamber due to the interaction between the amide groups on the molecular chain and the surrounding water molecules. Fig. 4(b) shows the humidity sensing process of absorbing water molecules around the sensor inside the humidity chamber. The wavelength shift of the reflection spectrum is monitored by setting different humidity levels. The sensor probe is sealed in the humidity chamber with the glass slide. Based on the experimental device in Fig. 4(c), the light spreads through circulator to one end of the fabricated sensor, and the reflection light was received at the terminal of the OSA.

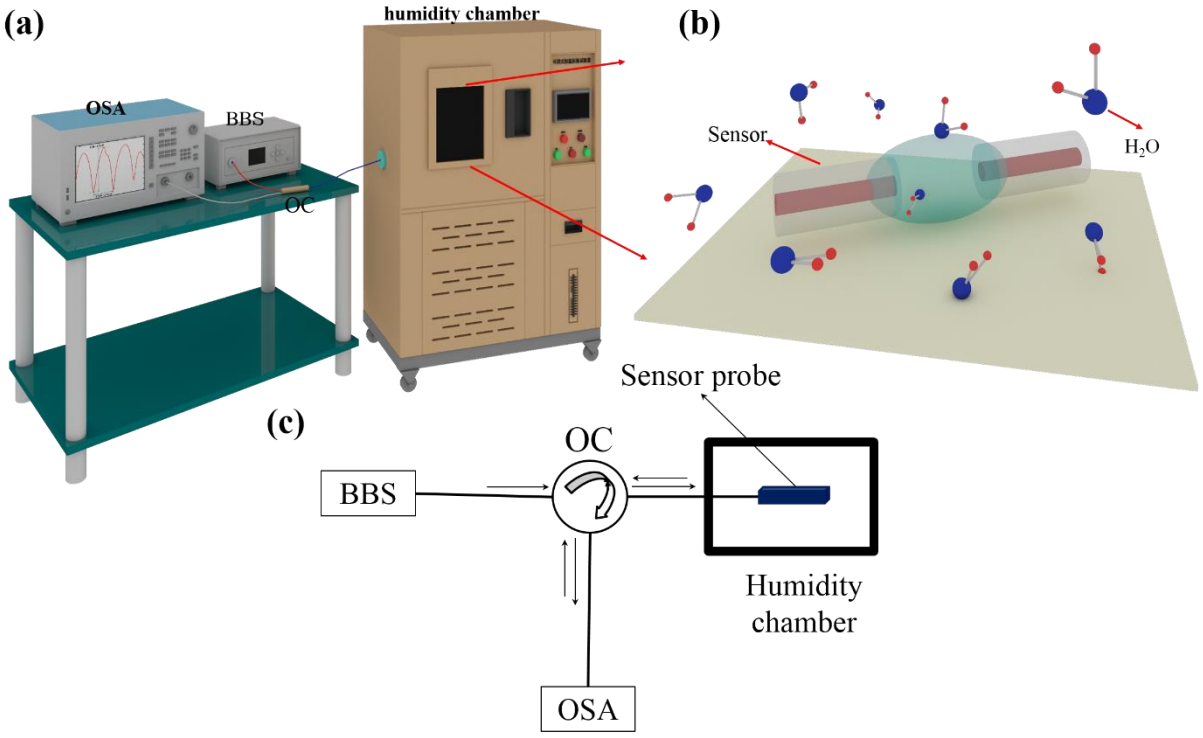

Fig. 4(a) Schematic diagram of humidity experimental test scene; (b) Humidity sensing process in the humidity chamber; (c) Schematic diagram of humidity experimental system.

After determining the appropriate cavity length and connecting the equipment, the data point of the reflection spectrum was obtained, which is dense enough to resolve the dense fringe and the extinction ratio (ER) and free spectral range (FSR) were obtained, as shown in Figure 5(a). The spatial frequency spectrum is obtained by processing the reflectance spectrum in Fig. 5(a) through Fast Fourier Transform (FFT). As revealed in Fig. 5(b), only the main peak whose frequency is in the range of 0-0.06125 Hz participates in the interference, while the other peaks have little influence.

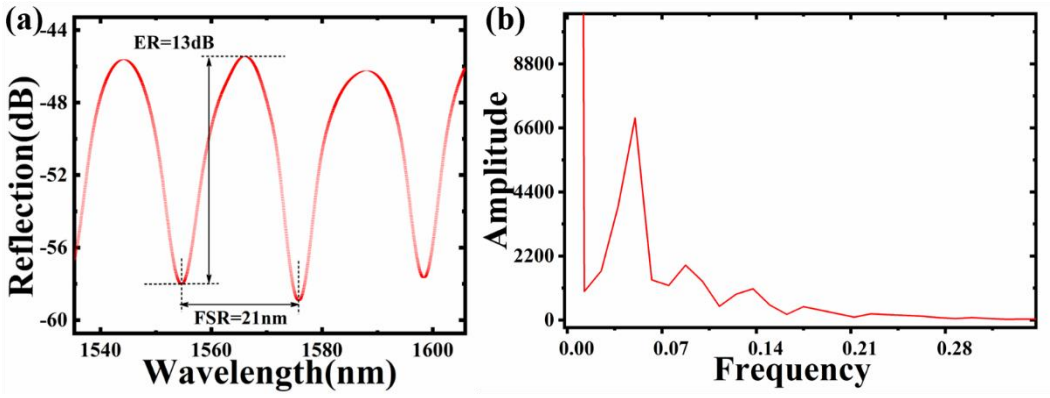

Fig. 5(a) Reflection spectrum of the FPI, where the cavity length d = 62.5 μm; (b) Fourier transform spatial spectrogram.

4.1 RH Sensitivity

For the sake of exploring the sensing characteristics of the sensitivity of the FP cavity, the RH sensor was tested under different humidity conditions by varying RH range from 45% to 75% with a step change of 5%RH. The measured spectral response at different RH level is shown Fig. 6(a). It can be observed that the wavelength generates bathochromic shift with RH increases and the summarized wavelength and RH is shown in Fig. 6(b). linear fitting of the measured results shows that the RH sensitivity of the sensor is 1.63629 nm/%RH and the linearity R^2 is 0.9897, which is 5.8 times higher than the optical fiber FPI RH sensor filled with hydrophilic chitosan materials[27], and 37.2 times higher than the RH sensor coated with hydrophilic agarose gels [28]. The influence

of PNIPAM hydrogel concentration on the sensor sensitivity has been studied and summarized wavelength shift and RH with different PNIPAM hydrogel concentration (8%. 10% and 12%) is shown in Fig. 6(c). The different concentrations of PNIPAM hydrogels were fabricated, as following: First, take an appropriate volume of 12% PNIPAM hydrogel, according to the formula $C_1V_1=C_2V_2$, where C_1 represents the concentration before dilution, V_1 represents the volume before dilution, C_2 represents the concentration after dilution, and V_2 represents the volume after dilution, add the calculated deionized water, and finally stir for 30 minutes and let stand to obtain the desired concentration. The experimental data show that the higher the PNIPAM hydrogel concentration, the higher the sensitivity of the sensor. When the PNIPAM hydrogel concentration increases from 8% to 12%, the RH sensitivity increases from 1.17307 nm/%RH to 1.63629 nm/%RH. The sensors shown good linear response at all three PNIPAM hydrogel concentration.

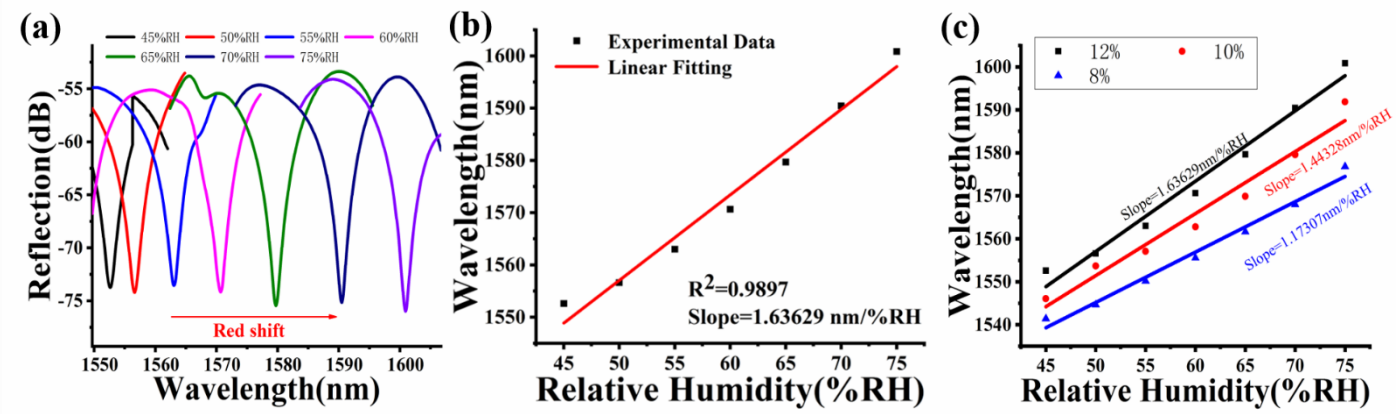

Fig. 6(a) Spectral response of FPI at a concentration of 12% PNIPAM in the range of 45%-75%RH; (b) Linear fitting of wavelength and relative humidity; (c) Linear fitting and sensitivity changes of different PNIPAM concentrations in the range of 45% ~ 75% RH.

4.2 Repeatability

The stability and repeatability of the fabricated sensor are also experimentally demonstrated. In a pre-programmed humidity chamber, as the RH is controlled by a programmer, the OSA records spectra every 15 seconds. The wavelength shift and time is plotted in Fig. 7(a). The results show that the measured sensor wavelength shifts and the preset RH values fairly consistent. Furthermore, for the sake of verifying the stability, the FPI sensor was placed inside the humidity chamber at a constant temperature of 20 °C and a constant 65% RH environment for 26 min, as shown in Fig. 7(b). It can be seen that the fluctuation of the wavelength shift in the humidity chamber is basically the same as that at room temperature, Due to the instability of humidity chamber itself, which has maximum error of 0.3%RH. In regard to discuss the reproducibility of the RH sensor, as shown in Fig. 7(c), three FPI sensors were fabricated with the same concentration of 8% PNIPAM and the same preparation parameters, denoted as W_0, W_1 and W_2, whose sensitivities were 1.17307 nm/%, respectively RH, 1.1754nm/%RH and 1.17672nm/%RH, it is observed that the reproducibility of the sensor is very good. In the RH range of 45% ~ 75%, the mean value of wavelength drift of the three sensors with 8% PNIPAM is analyzed and processed, as shown in Fig. 7(d), which exhibits a small error bar with a sensitivity of 1.19136nm/ %RH is in good agreement with experimental data.

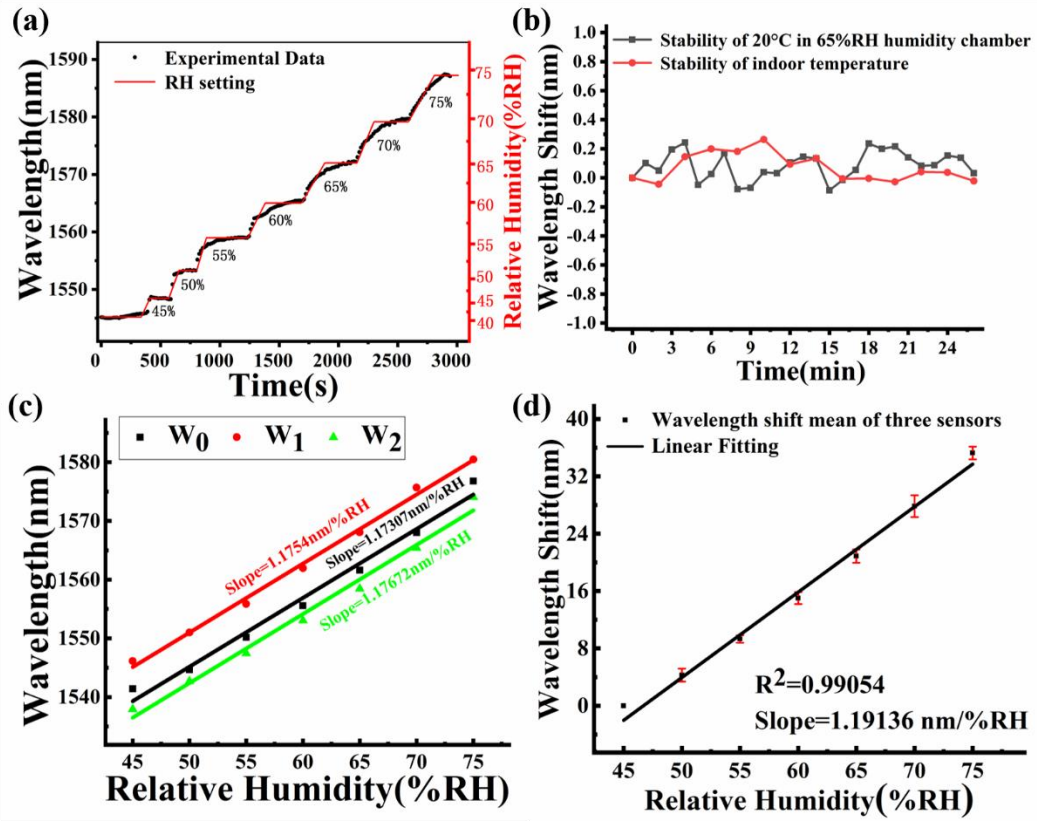

Fig. 7(a) Trough wavelength as a function of time; (b) Monitoring of sensor stability at a constant temperature of 20 °C (65% RH) and room temperature; (c) Linear fit and sensitivity of 3 sensors to 8% PNIPAM in the range of 45% to 75% RH; (d) Wavelength drift mean and error bars of three sensors for the same concentration of 8% PNIPAM.

4.3 Respiratory monitoring

The normal and medically diagnosed respiratory rate for a healthy person is 12 to 22 breaths per minute, and one breath is about 2.73 to 5 seconds, which has been demonstrated by a wearable sensor for respiration monitoring using an intensity variation-based approach in D-shape SMF [34]. Our developed FPI sensor is applied to real respiratory monitoring. Figures 8(a) and (b) show the practical and schematic diagram of the experimental setup respectively at room temperature. The optical signal is detected by the photodetector (PD; THORLABS, PDA10CS2) and collected by a field programmable logic gate array (FPGA; Wuhan Xinluheng Technology Co. Ltd. AC620), which sampling interval is set to 100ms. Figure 8(c) shows the picture of a fabricated fiber-optic FPI sensor attached on a breath mask, and Fig. 8(d) is a picture of a commercial sensor (Hefei Huake Information Technology Co. Ltd. HKH-11C) worn on a volunteer's waist for respiratory test. Figure 8(e) shows the respiration response of the fabricated fiber-optic FPI sensor and a commercial breathing sensor at room temperature. Figure 8(f) is zoom in of the respiratory response monitored by the fabricated FPI sensor, which show that during exhalation, the amplitude immediately rises sharply and then remains in a steady state for a short period. During inhalation, the monitored amplitude drops suddenly. Response and recovery time are 0.91 s and 1.91 s, respectively. The increase in humidity during exhalation causes the geometry expand of the PNIPAM hydrogel in the sensor and increase of the effective refractive index, and the inhalation process results in the evaporation of water molecules, and thus shrink of the PNIPAM hydrogel. The response measure by our sensor has similar response to that of commercial sensor shown in Fig. 8(g), although the operating principle is different. The recovery time measured during breath detection was much faster than the response time in earlier humidity experiments. This is because the airflow velocity is affected by exhalation and inhalation, thereby changing the humidity in the mask more quickly and accelerating the evaporation of water

molecules within the coating [35]. Finally, Table 1 is obtained by comparing the performance of fiber-optic humidity sensors with different structures and humidity-sensitive materials.

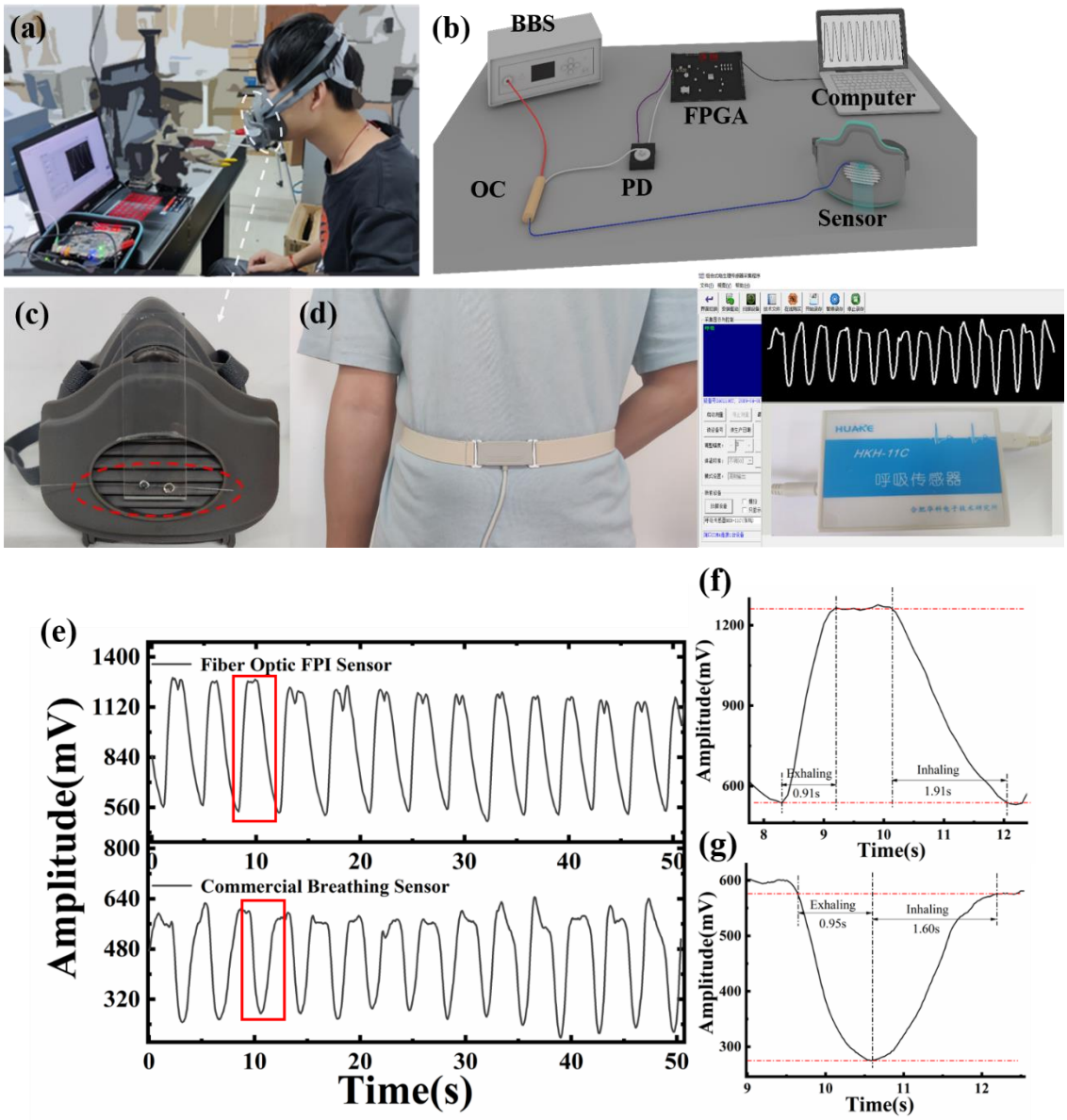

Fig. 8 (a) The scene diagram of the breathing experiment; (b) The schematic diagram of the experiment for response time detection; (c) The picture of a fabricated fiber-optic FPI sensor attached on a breathing mask; (d) The scene diagram of a commercial breathing sensor worn on a volunteer's waist for respiratory response testing; (e) The respiratory response testing of comparing the respiration response of the fabricated fiber-optic FPI sensor with a commercial breathing sensor; (f) partial enlarged view of the respiratory response monitored by the fabricated FPI sensor; (g) a commercial breathing sensor monitor the partial enlarged view of the respiration response.

Table I：Comparison with other fiber-optic humidity sensors.

Sensing structure	Sensing material	Sensitivity	Response & Recovery times(s)	References
FPI	Ti_3O_5/SiO_2	0.43nm/%RH	5，5	[29]
FPI	PVA	36.71pm/%RH	1.5, 2.5	[1]

FPI	Chitosan	0.13nm/%RH	0.38，—	[30]
Microfiber Sagnac interferometer	No coating	201pm/% RH	0.06 , —	[31]
Michelson Interferometric	Gelatin-Coated	0.145nm/%RH	5.24 , 7.14	[32]
Micro-nano Fiber Bragg Grating	Graphene oxide	-0.185 nm/%RH	3.2, 8.3	[33]
FPI	PNIPAM gel	1.636nm/%RH	0.91, 1.91	This work

5. Conclusion

In this work, PNIPAM hydrogel was utilized as a RH sensing material coated on the gap between the ends of two SMFs, which an optical fiber FP humidity sensor was formed. This PNIPAM hydrogel has amido groups of hydrophilic, and can absorb water molecules, of which its RI is dependent on RH. Experimental study indicated that the sensitivity of the RH sensor was 1.63429 nm/%RH in the RH range of 45%–75%. In addition, the sensitivity of sensor is PNIPAM hydrogel concentration dependent: the higher the concentration, the higher the sensitivity. The developed sensor has a response to detect human respiratory with response and recovery time of 0.91 s and 1.91 s, respectively. The developed sensor has the merits of high sensitivity, excellent stability and reproducibility, simple fabrication, and low expense, which make it have a bright prospect in practical applications of fiber-optic humidity sensors.

Acknowledgements

This work was jointly supported by the Natural Science Foundation of Jiangxi Province (20212BAB202024), National Natural Science Foundation of China (NSFC) (11864025, 62163029, 62175097 and 62065013). Nanchang Hangkong University graduate student innovation special fund project (Grant No. YC2021-074).

References

[1] N. Wang, H. Zhang, X. Yu, Optical Fiber Fabry–Perot Humidity Sensor Filled with Polyvinyl Alcohol, Sensors and Materials, 3 (2021) 1051. https://doi.org/10.18494/SAM.2021.3229

[2] Q Wu, Y Semenova, J Mathew, P Wang and G Farrell, Humidity sensor based on a single-mode hetero-core fiber structure, Optics Letters, 36 (2011) 1752-1754. https://doi.org/10.1364/OL.36.001752.

[3] Erwin Maciak. Low-Coherence Interferometric Fiber Optic Sensor for Humidity Monitoring Based on Nafion® Thin Film, Sensors. 3 (2019). https://doi.org/10.3390/s19030629.

[4] C. Lang, Y. Liu, K. Cao, Ultra-compact, fast-responsive and highly-sensitive humidity sensor based on a polymer micro-rod on the end-face of fiber core, Sensors and Actuators B: Chemical, 290 (2019) 23-27. https://doi.org/10.1016/j.snb.2019.03.099

[5] B. Wang, J. Tian, L. Hu and Y. Yao, High Sensitivity Humidity Fiber-Optic Sensor Based on All-Agar Fabry–Perot Interferometer, IEEE Sensors Journal, 12 (2018) 4879-4885. https://doi.org/10.1109/JSEN.2018.2828134.

[6] L. Chen, B. Liu, J. Liu, U-Shape Panda Polarization-Maintaining Microfiber Sensor Coated With Graphene Oxide for Relative Humidity Measurement, Journal of Lightwave Technology, 19 (2021) 6308-6314. https://doi.org/10.1109/jlt.2021.3096505.

[7] C. Li, X. Yu, W. Zhou, Ultrafast miniature fiber-tip Fabry–Perot humidity sensor with thin graphene oxide diaphragm, Optics Letters, 19 (2018). https://doi.org/10.1364/OL.43.004719.

[8] P. Li, H. Yan, Z. Xie, A bandwidth response humidity sensor with micro-nano fiber Bragg grating, Optical Fiber Technology, 53 (2019) 101998. https://doi.org/10.1016/j.yofte.2019.101998.

[9] Q Wu, Y Semenova, P Wang, G Farrell, High sensitivity SMS fiber structure based refractometer - analysis and experiment, Optics Express, 19 (2011): 7937-7944. https://doi.org/10.1364/OE.19.007937.

[10] Q. Wu, Y. W. Qu, J. Liu, Singlemode-Multimode-Singlemode fiber Structures for Sensing Applications - A Review, IEEE Sensors Journal, 21 (2021) 12734-12751. https://doi.org/10.1109/JSEN.2020.3039912.

[11] T. Gong, X. Liu, Z. Wang and Y. Liu. A highly sensitivity humidity sensor based on mismatching fused fiber Mach–Zehnder interferometric without moisture material coating, Journal of Optics, 2 (2020) 025801-9. https://doi.org/10.1088/2040-8986/ab6426.

[12] A. M. Shrivastav, D. S. Gunawardena, Z. Liu, Microstructured optical fiber based Fabry–Pérot interferometer as a humidity sensor utilizing chitosan polymeric matrix for breath monitoring, Scientific Reports, 10 (2020) 1-10. https://doi.org/10.1038/s41598-020-62887-y.

[13] Y. Wang, Y. Liu, F. Zou, Humidity Sensor Based on a Long-Period Fiber Grating Coated with Polymer Composite Film, Sensors, 19 (2019) 2263. https://doi.org/10.3390/s19102263.

[14] X. Sun, H. Gong, M. Xie and C. Zhao. All-fiber humidity sensor based on Michelson interferometer with hyaluronic acid and polyvinyl alcohol composite film – ScienceDirect, Optical Fiber Technology, 60 (2020) 102381. https://doi.org/10.1016/j.yofte.2020.102381.

[15] Z. Li, B. Dong, E. Chen, High sensitivity FBG humidity sensor coated with graphene and polyimide films, Optical Fiber Technology, 66 (2021): 102635. https://doi.org/10.1016/j.yofte.2021.102635.

[16] T. Sun; W. Wang; J. Peng, Effect of Different Inorganics on Polyimide-Based Bragg Grating Humidity Sensor, IEEE Sensors Journal, 19 (2019) 2016-2022. https://doi.org/10.1109/JSEN.2018.2885126.

[17] P. Dey and E. L. Izake, Mixed Polymer-Coated Magnetic Nanoparticles as Forward Osmosis Draw Agents of Tuned Hydrophilicity, Chemistry-A European Journal, 22 (2016): 11253-11260. https://doi.org/10.1002/chem.201600144.

[18] Z. Dai, S. Zhao and Y. Xue. Temperature-sensitivity of PU/PNIPAM semi-IPN microporous membranes, Acta Polymerica Sinica, 5 (2012) 508-512. https://doi.org/10.3724/sp.j.1105.2012.11418.

[19] Y. Pan, Q. Wu, Y. Weng, Declined ionic flux through the nano-pores of vertically aligned carbon nanotubes filled with PNIPAm hydrogel, Journal of Materials Chemistry A, 3 (2015) 11111-11116. https://doi.org/10.1039/C5TA01749A.

[20] M. Zhernenkov, R. Ashkar, H. Feng, Thermoresponsive PNIPAM coatings on nanostructured gratings for cell alignment and release, ACS applied materials & interfaces, 7 (2015) 11857-11862. https://doi.org/10.1021/acsami.5b01453.

[21] S. Ashraf, H. Park, H. Park, and S. Lee. Snapshot of phase transition in thermoresponsive hydrogel PNIPAM: Role in drug delivery and tissue engineering, Macromolecular Research 4 (2016) 297-304. https://doi.org/10.1007/s13233-016-4052-2.

[22] X. Li and X. Su. Multifunctional smart hydrogels: potential in tissue engineering and cancer therapy, Journal of Materials Chemistry B 6 (2018) 4714. https://doi.org/10.1039/C8TB01078A.

[23] W. Chen, X.. Lei, W. Zhang, X. Liu and C. Liao. Recent Progress of Optical Fiber Fabry-Perot Sensors, Acta Optica Sinica, 38 (2018) 0328010. https://doi.org/10.3788/AOS201838.0328010.

[24] C. Lee and M. S. Strano. Understanding the Dynamics of Signal Transduction for Adsorption of Gases and Vapors on Carbon Nanotube Sensors, Langmuir the Acs Langmuir, 11 (2005) 5192. https://doi.org/10.1021/la046867i.

[25] C. Yu, Y. Wu, X. Liu, Yu, Miniature fiber-optic NH_3 gas sensor based on Pt nanoparticle-incorporated graphene oxide, Sensors and Actuators B: Chemical, 244 (2017) 107-113. https://doi.org/10.1016/j.snb.2016.12.126.

[26] Y. Hu, L. Barbier, Z. Li, Making Hydrogels Stronger through Hydrophilicity-Hydrophobicity Transformation, Thermoresponsive Morphomechanics and Crack Multifurcation. 33 (2020). https://doi.org/10.26434/chemrxiv.12279686.v1.

[27] X. Liu, M. Jiang, Q. Sui and X. Geng, Optical fibre Fabry–Perot relative humidity sensor based on HCPCF and chitosan film, Journal of Modern Optics, 17 (2016) 1668-1674. https://doi.org/10.1080/09500340.2016.1167974.

[28] S. Novais, M. S. Ferreira and J. L. Pinto. Relative Humidity Fiber Sensor Based on Multimode Interferometer Coated with Agarose-Gel, Coatings, 12 (2018). https://doi.org/10.3390/coatings8120453.

[29] W. Xie, M. Yang, Y. Cheng, Optical fiber relative-humidity sensor with evaporated dielectric coatings on fiber end-face, Optical Fiber Technology, 4 (2014) 314-319. https://doi.org/10.1016/j.yofte.2014.03.008.

[30] L. H. Chen, T. Li, C. C Chan, Chitosan based fiber-optic Fabry–Perot humidity sensor, Sensors and Actuators B: Chemical 169 (2012) 167-172. https://doi.org/10.1016/j.snb.2012.04.052.

[31] L. Sun, J. Li, L. Jin, High-birefringence microfiber Sagnac interferometer based humidity sensor, Sensors and Actuators B: Chemical, 231 (2016) 696-700. https://doi.org/10.1016/j.snb.2016.03.102.

[32] Y. Liu, A. Zhou, L. Yuan, Gelatin-Coated Michelson Interferometric Humidity Sensor Based on a Multicore Fiber With Helical Structure, Lightwave Technology Journal of, 10 (2019) 2452-2457. https://doi.org/10.1109/JLT.2019.2907568.

[33] M Tian, Y Huang, C Li, High-performance Humidity Sensor Based on Micro-nano Fiber Bragg Grating Coated with Graphene Oxide, Optics Express, 28 (2020) 26395-26406. https://doi.org/10.1364/OE.402648.

[34] J. Li, B. Liu, J. Liu, et al. Low-cost wearable device based D-shaped single mode fiber curvature sensor for vital signs monitoring, Sensors and Actuators A: Physical, 337 (2022). 113429. https://doi.org/10.1016/j.sna.2022.113429.

[35] Y. T Yi, Y. X Jiang, H. Y Zhao, et al. High-Performance Ultrafast Humidity Sensor Based on Microknot Resonator-Assisted Mach-Zehnder for Monitoring Human Breath, ACS Sensors, 5 (2020) 3404–3410. https://doi.org/10.1021/acssensors.0c00863.